Open Archive Toulouse Archive Ouverte (OATAO)

OATAO is an open access repository that collects the work of Toulouse researchers and makes it freely available over the web where possible.

Any correspondence concerning this service should be sent to the repository administrator: staff-oatao@inp-toulouse.fr

The Zr–Sn binary system: New experimental results and thermodynamic assessment

R. Jerlerud Pérez [a,*], C. Toffolon-Masclet [b], J.-M. Joubert [c], B. Sundman [d]

[a] *Division of Computational Thermodynamics, Department of Materials Science and Engineering, Royal Institute of Technology, 100 44 Stockholm, Sweden*
[b] *Division of Applied Research in Metallurgy, Department of Nuclear Materials, CEA Saclay, 91191 Gif-sur-Yvette, France*
[c] *Chimie Métallurgique des Terres Rares, Institut de Chimie et des Matériaux Paris-Est, CNRS, 2-8 rue Henri Dunant, 94320 Thiais, France*
[d] *CIRIMAT, UPS/INPT/CNRS ENSIACET, 31077 Toulouse, France*

ABSTRACT

The Zr–Sn binary system has been reinvestigated by several experimental techniques: X-ray diffraction, electron probe micro-analysis, mass density and calorimetry measurements. The existence of a miscibility gap inside the homogeneity domain of the η phase (Zr_5Sn_3–Zr_5Sn_4) has been confirmed. It has been also shown that Zr substitution on the Sn sublattice is responsible for the non-stoichiometry of the $A15$ phase (Zr_4Sn). The temperature of the peritectoid reaction $\beta_{Zr}+A15 \leftrightarrow \alpha_{Zr}$ has been determined to be at 1216 K that is 40° below the temperature reported in the literature. All these new experimental data have been taken into account for a new thermodynamic assessment of this system.

1. Introduction

Zirconium alloys containing Sn (1.2%–1.7% Sn) and small amounts of Cr, Fe, Ni and O are widely used as fuel cladding in nuclear reactors. In the further development of these alloys, computational thermodynamics has shown its efficiency for studying and designing complex alloys. In order to perform such thermodynamic calculations, it is necessary to describe the Gibbs energy of each phase of the binary systems constituting an alloy. Descriptions of low order systems can then be combined in order to make extrapolations to higher order systems. There are unclear features concerning the phase equilibria in important binary systems such as Zr–Fe and Zr–Sn for instance. This work aims aims to improve this last system by means of experimental determinations and thermodynamic calculations.

The published experimental information on the Zr–Sn binary system is scarce and, to some extent, uncertain. The phase diagram has been studied experimentally by Mc Pherson and Hansen [1], Speich and Kulin [2], Carpenter et al. [3], Arias and Roberti [4], Kwon and Corbett [5–7].

This binary system has already been assessed by different authors [8–12]. However, some disagreements remain among the different studies. In order to increase the knowledge of this system and to present an improved thermodynamic assessment, a combined theoretical and experimental work has been performed. The theoretical work deals with first-principles calculations of the enthalpy of formation of the intermetallic compounds as reported by Baykov et al. [13]. The experimental work was aimed at studying the intermetallic phases and more specifically the region Zr_5Sn_3–Zr_5Sn_4 and the Zr_4Sn phase. In particular, the range of existence of these two phases as well as the nature of the crystallographic defects responsible for the non-stoichiometry was studied. This made it possible to select an appropriate sublattice model for each phase in the frame of the Calphad modeling. In addition, the temperature of the peritectoid reaction $\beta_{Zr} + Zr_4Sn \leftrightarrow \alpha_{Zr}$ was redetermined by differential scanning calorimetry (DSC).

The system was optimized using the Calphad method. A final consistent set of parameters has been obtained with good agreement between calculated and available experimental data.

* Corresponding address: Product and Material Analysis, Rolled Product Division, Luvata Sweden AB. P.O. Box 550, Skivfilargränd 3 SE-721 10 Västerås, Sweden. Tel.: +46 21198637; fax: +46 21198035.

E-mail addresses: rosa@mse.kth.se, Rosa.JerlerudPerez@Luvata.com
(R. Jerlerud Pérez).

2. Available experimental information

2.1. Phase diagram and thermodynamic data

In Ref. [1] metallographic studies of arc-melted and annealed samples were performed in a temperature interval from 873 to 1773 K, combined with thermal analysis and X-ray diffraction (XRD). The authors established the main features of the Zr–Sn binary phase diagram: the Zr_4Sn phase (20 at.% Sn) is formed by the peritectoid reaction $\beta_{Zr}(bcc) + Zr_5Sn_3 \leftrightarrow Zr_4Sn$ at 1598 ± 20 K. A stoichiometric intermetallic compound Zr_5Sn_3 (37 at.% Sn) was observed. It melts congruently at 2258 ± 25 K and is formed together with β_{Zr} from a liquid with 23.5 at.% Sn in a eutectic reaction at 1863 ± 15 K. At 1253 K a peritectoid reaction $\beta_{Zr} + Zr_4Sn \leftrightarrow \alpha_{Zr}$ (hcp) takes place. From this invariant reaction the solubility of Sn in α_{Zr} decreases from 7.06 at.% to 1.15 at.% Sn at 873 K.

The $\alpha_{Zr}/(Zr_4Sn)$ boundary was reinvestigated in Refs. [2–4]. By means of X-ray lattice parameter determinations of strain aged, heat treated and quenched alloys, Speich et al. [2] studied the Sn solubility in α_{Zr} between 573 and 1173 K. The results are in relative agreement with the ones reported in Ref. [1].

On the other hand, in the work of Carpenter et al. [3], the $\alpha_{Zr}/(Zr_4Sn)$ boundary was observed at higher Sn content than in previous work. The samples, containing 1.15–7 at.% Sn, were examined by means of optical and electron microscopy, hardness and XRD. In the alloys which were solution pre-treated and aged for long time (1000 h) at temperatures ranging from 773 to 1073 K, little or no precipitation of Zr_4Sn was observed, suggesting that the Sn solubility in α_{Zr} is higher than that reported in the previous studies [1,2].

Arias et al. [4] reinvestigated the Zr rich side below 1273 K. The experimental techniques used were optical and electron microscopy, electrical resistivity and electron probe micro-analysis (EPMA). The α_{Zr} solvus is in relative agreement with Ref. [1,2] and in disagreement with the larger solubility reported in Ref. [3]. More recently, in the work performed by Toffolon et al. [14], the solubility limit of Sn in α_{Zr} has been measured by EPMA and evaluated by means of first-principles calculations using the CASTEP code. In the experimental studies, samples with a nominal composition 10 at.% Sn were annealed at four different temperatures: 1173, 1073, 973 and 873 K. After each thermal treatment, the microstructure showed two phases in equilibrium: α_{Zr} and Zr_4Sn. The measured Sn solubility limit in α_{Zr} decreased from 6.4 at.% Sn at 1173 K to 5.4 at.% Sn at 873 K. On the other hand, the calculated one decreased from 6.0 at.% Sn at 1173 K to 4 at.% Sn at 673 K. Both results are in fairly good agreement with each other and with Ref. [3], but in disagreement with some of the previous works [1,2].

Concerning thermodynamic properties, liquid Zr–Sn alloys were studied by means of isoperbolic calorimetry at 1873 K by Valishev et al. [15] and at 1889 K by Sudatsova and Batalin [16]. In the work by Valishev et al. the experiments were carried out in an alumina calorimetric crucible in an atmosphere of spectral pure helium. The zirconium partial enthalpy of mixing $\Delta \bar{H}_{Zr}$ was measured within a concentration range up to 31.6 at.% Zr in Ref. [15] and up to 40 at.% Zr in Ref. [16]. As we will see later, the results of these two studies differ significantly.

For the intermetallic compounds, the enthalpy of formation of the compound Zr_5Sn_3, has been measured by means of direct reaction calorimetry (DRC) at 1473 ± 2 K by Meschel and Kleppa [17] and calculated by Baykov et al. [13] using first-principles (FP).

2.2. The Zr_4Sn-A15 phase

In Ref. [1], a tetragonal structure and the stoichiometry Zr_4Sn were assigned to this phase. In Ref. [14,18,19], it was concluded from XRD studies that this compound has the $A15$ cubic structure, isotypic with Cr_3Si, and the composition Zr_3Sn was given. Kwon and Corbett [5] confirmed the cubic $A15$ structure but noticed the difference between the actual (4:1) and the ideal (3:1) stoichiometries. Two mechanisms were proposed to explain the non-stoichiometry: presence of Sn vacancies ($Zr_3(Sn_{.75}Va_{.25})$) or Zr substitution on the Sn site ($Zr_3(Sn_{.8}Zr_{.2})$). However, the authors had no experimental evidence to choose between the two models. In addition, a solubility range has been observed in this phase, Arias and Roberti [4] measured a composition of 17.6 ± 1.3 at.% Sn by EPMA in a sample annealed at 1223 K for 540 h. Kwon and Corbett [6] also reported a small composition variation in arc-melted samples annealed at 1273 K for 168 h. The results obtained in this work (Section 3) provide additional data about the composition range of this phase.

To avoid the confusion between its name and its composition, this phase will be designated as 'the $A15$ phase' in the following.

2.3. The η phase

The intermetallic compound Zr_5Sn_3 was reported in Ref. [1] as stoichiometric with the hexagonal Mn_5Si_3 structure type. Grand and Andersson [18] reported two stoichiometric phases with a hexagonal lattice: Zr_5Sn_3' and Zr_5Sn_3'', the second one having a larger unit cell and higher Sn content.

Kwon and Corbett [5,6] clarified the situation by assigning compositions and structure types to the two previously reported phases. The phase at the composition Zr_5Sn_3 has the Mn_5Si_3 structure type while the phase at the composition Zr_5Sn_4 has the Ti_5Si_4 structure type. The two crystal structures are strongly related. They have the same space group ($P6_3/mmc$) and the same occupied sites and positions for most atoms. They differ only by the full occupancy of the Wyckoff position $2b$ by Sn in the case of Zr_5Sn_4, while this site is completely unoccupied in the case of Zr_5Sn_3. Of course, the cell volume is larger in the former case. Additionally, these authors claim that a single phase domain exists at high temperature between these two compositions so that the phase can be described as $Zr_5Sn_{3+x} (0 \leq x \leq 1)$, x being the occupancy parameter in site $2b$. The phase melts congruently at 2263 K and $x = 0.3$. A rather surprising feature was observed below 1773 K where a miscibility gap forms inside the homogeneity range of the intermetallic phase giving rise to equilibrium between the two compositions Zr_5Sn_4 and Zr_5Sn_3. To avoid confusion between the phase and its compositions, it will be named η in the following. In Section 3, we will confirm the presence of the miscibility gap and give new results regarding its homogeneity range.

3. Experimental work

3.1. Experimental details

All the experiments have been performed in the Zr rich side of the phase diagram. The details about annealing treatments are summarized in Table 1.

The alloys (3–5 g) were arc melted from the pure elements under high purity argon. Zirconium was provided as crystal bar (Zr Van Arkel) and spectral pure Sn from Johnson Mattey. In order to study the region Zr_5Sn_4–Zr_5Sn_3 previously investigated in the literature, four alloys were synthesized: an alloy with 34 at.% Sn located in the two phase domain $A15 + \eta$, two alloys at the nominal compositions 41 at.% Sn and 40 at.% Sn (between the compositions Zr_5Sn_3 and Zr_5Sn_4), and, finally, an alloy containing 49 at.% Sn

Table 1
Metallurgical characterization of the samples studied in this work

Composition	Heat treatment (T (K) / time (h))	Phases	Amount (wt.%)	Lattice parameters (Å) (± 0.001)	Refined composition (XRD) (± 0.3 at.%)	Analyzed composition (EPMA)
$Zr_{80}Sn_{20}$	1273 / 288	$A15$	92	$a = 5.625$	$Zr_{78.3}Sn_{21.7}$	$Zr_{81.2(1)}Sn_{18.8(1)}$
		η	3	$a = 8.450$	–	$Zr_{64.7(5)}Sn_{35.3(5)}$
				$c = 5.786$		
		α_{Zr}	5	$a = 3.216$	–	–
				$c = 5.154$		
$Zr_{66}Sn_{34}$	1273 / 216	$A15$	19	$a = 5.627$	–	$Zr_{81.0(3)}Sn_{19.0(3)}$
		η	81	$a = 8.470$		$Zr_{64.2(3)}Sn_{35.8(3)}$
				$c = 5.787$		
$Zr_{60}Sn_{40}$	1873 / 6	η	100	$a = 8.524$	$Zr_{60.8}Sn_{39.2}$	–
				$c = 5.833$		
$Zr_{59}Sn_{41}$	1273 / 216	η(Sn poor)	18	$a = 8.452$	–	–
				$c = 5.772$		
		η(Sn rich)	82	$a = 8.589$	$Zr_{58.8}Sn_{41.2}$	–
				$c = 5.870$		
$Zr_{51}Sn_{49}$	1273 / 216	η	80	$a = 8.765$	$Zr_{55.6}Sn_{44.4}$	
				$c = 5.933$	–	
		$ZrSn_2$	20	$a = 5.643$		
				$b = 9.574$		
				$c = 9.927$		

in the two phase domain η + $ZrSn_2$. The two alloys in the two phase domains were selected to study the η phase at its richest and poorest Zr compositions. To study the $A15$ phase, an alloy with 20 at.% Sn was synthesized. In none of the samples, weight losses exceeded ~1%. The annealing was performed under argon in a silica tube. In order to avoid any reaction with the silica the alloys were protected with Ta foils. The sample with the nominal composition 20 at.% Sn was annealed for 240 h at 1273 K. The samples, which contained 34, 41 and 49 at.% Sn, were annealed for 216 h at 1273 K. After the annealing treatment the alloys were quenched in water at room temperature. The sample containing 40 at.% Sn was annealed for 6 h at 1883 K in an induction furnace in a cold copper crucible under argon atmosphere and quenched by turning off the induction power. This annealing treatment was performed in order to check the closure of the miscibility gap. DSC experiments were performed on a sample with 10 at.% Sn previously thermally treated at 1073 K during 680 h.

XRD measurements were carried out in a D8 Advance (Bruker) high resolution powder diffractometer, using Bragg–Brentano geometry, with Cu Kα radiation. The sample was previously reduced into fine powder in an agate mortar. The chemical quantitative analysis by EPMA on polished samples was obtained using a Cameca SX100 with a wavelength dispersive spectrometry analysis system. The mass density equipment consists of a helium gas pycnometer Micromeritics (AccuPyc 1330). DSC measurements were performed with a Setaram Multi HTC high-temperature high-sensitivity calorimeter. The experiments were conducted under inert gas (pure argon or helium) with samples of mass 1 g, for typical heating/cooling rates ranging from 3 K/min up to 10 K/min.

Phase identification, quantification, lattice parameters and site occupancies were obtained with the full pattern Rietveld refinement of XRD data and supported by EPMA measurements.

3.2. Results and discussion

The experimental results regarding XRD and EPMA measurements are summarized in Table 1.

3.2.1. The A15 phase

The chemical composition after annealing of the $A15$ phase in the sample $Zr_{80}Sn_{20}$ was 18.8 at.% Sn. The Rietveld refinement to the XRD data is given in Fig. 1. The quantification gives 92% of $A15$ phase, 3 wt.% of the η phase and 5 wt.% of α_{Zr}. The refinement of the
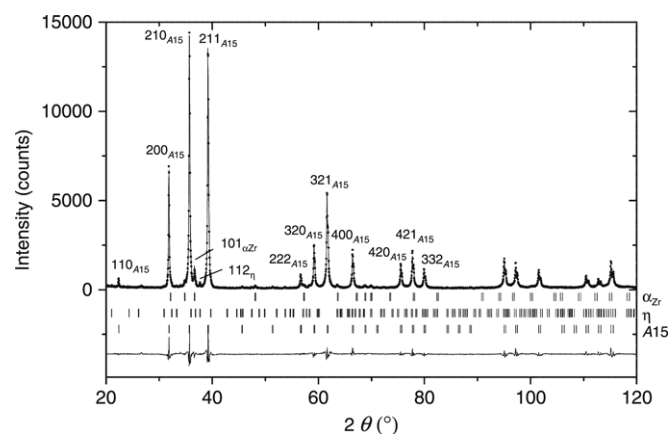

Fig. 1. XRD diagram and Rietveld refinement plot for the sample $Zr_{80}Sn_{20}$. The observed (dots), calculated (line) and difference (line below) patterns are shown. The ticks represent the reflections of the phases as indicated.

site occupancy parameters was constrained in order to match the measured composition of the $A15$ phase. The substitutional model ($Zr_3(Zr_{0.2}Sn_{0.8})$) gives an agreement factor between observed (I_{obs}) and calculated (I_{cal}) intensities $R_B = \frac{\sum I_{obs} - I_{cal}}{\sum I_{obs}} = 3.2\%$ (summation done over all reflections) while the vacancy model ($Zr_3Sn_{0.75}$) gives an agreement factor $R_B = 8.0\%$.

In the sample $Zr_{90}Sn_{10}$ annealed at 1073 K and 1173 K studied in Ref. [14], the composition of the $A15$ phase was found to be equal to 20.3 at.% Sn and 20.4 at.% Sn, respectively.

The measured density of the $A15$ phase (corrected from the presence of the additional phases) was 7.20 g/cm³. This result is in good agreement with the measured density in Ref. [5]: 7.10 g/cm³. It may be compared with the calculated density obtained for the substitutional ($Zr_3(Zr_{0.2}Sn_{0.8})$: 7.22 g/cm³) and for the vacancy model ($Zr_3Sn_{0.75}$: 6.77 g/cm³).

Thus, both XRD and mass density measurements are in favour of the substitutional model. The crystal structure data of the $A15$ phase are listed in Table 2.

3.2.2. The η phase

In the analysis of the XRD patterns, the Sn occupancy on the crystallographic site 2b was refined freely in most cases. Zero occupancy of this site yields Zr_5Sn_3 composition while full occupancy yields Zr_5Sn_4. The samples richest in Sn could not be analyzed by EPMA because of incredibly strong reaction with any

Table 2
Crystal structure data of the A15 and η phases

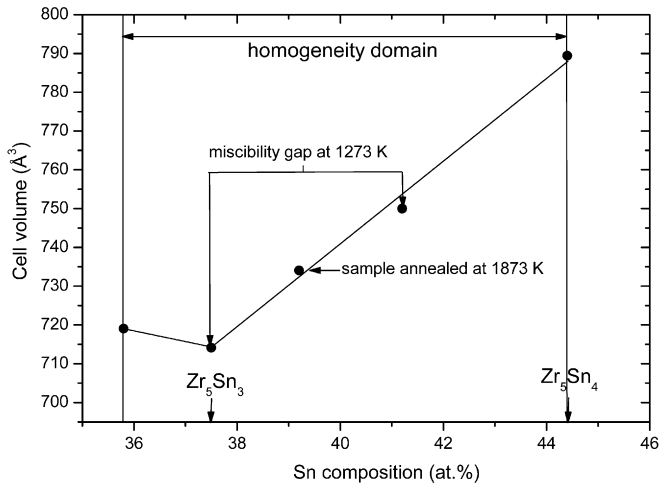| Wyckoff position	x	y	z	Occupancy
*A*15 phase, space group $Pm\bar{3}n$, No. 223				
2*a*	0	0	0	Sn, Zr
6*c*	1/4	0	1/2	Zr
η phase, space group $P6_3/mcm$, No. 193				
2*b*	0	0	0	Sn, Va
6*g*	$x_{Sn} \sim 0.61$	0	1/4	Sn
4*d*	1/3	2/3	0	Zr
6*g*	$x_{Zr} \sim 0.25$	0	1/4	Zr

Fig. 2. Cell volume of the η phase as a function of tin composition

of the water free polishing liquids we could find. The results of the characterization of the different samples are summarized in Table 1.

The sample with 49 at.% Sn shows, as expected from the phase diagram proposed by Kwon and Corbett [5], the equilibrium between the η phase and ZrSn$_2$. The refinement of the occupancy parameters indicates that the composition of the η phase is very close to Zr$_5$Sn$_4$ (44.4 at.% Sn).

We could also reproduce the results of these authors concerning the presence of a miscibility gap inside the range of existence of the η phase. Indeed, a peak splitting characteristic of the presence of two composition sets was evidenced in the sample with 41 at.% Sn annealed at 1273 K. However, the composition refined for the Sn richest phase (Zr$_5$Sn$_{3.5}$) was somewhat different from the one proposed by Kwon and Corbett [5](Zr$_5$Sn$_4$), indicating that the miscibility gap is not symmetric. This result is supported by three independent measurements:

- the refinement of the occupancy parameter on site 2*b* yielding the composition Zr$_5$Sn$_{3.5}$ instead of Zr$_5$Sn$_4$.
- the lattice parameters which are much smaller than the ones observed for Zr$_5$Sn$_4$ composition in the sample with 49 at.% Sn indicating a lower Sn content. In Fig. 2, one may see that the composition refined from XRD is in perfect agreement with Vegard's law applied to the other samples.
- the phase amount obtained from the refinement of XRD data. The application of the lever rule indicates that the nominal composition (Zr$_5$Sn$_{3.47}$) is very close to the Sn rich composition set.

It was not possible to refine the Sn content for the Sn poor phase but from the lattice parameter measurement, the composition should be close to Zr$_5$Sn$_3$.

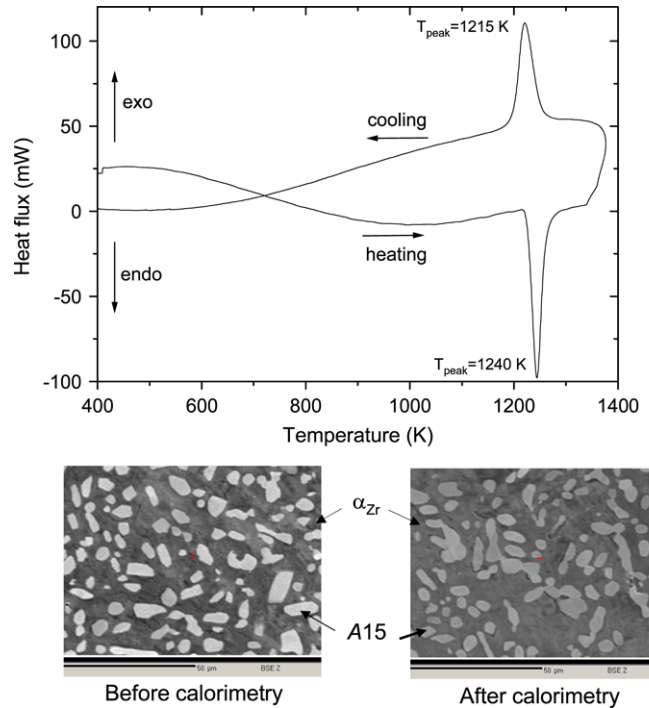A sample of approximately the same composition (40 at.% Sn) was annealed at 1873 K and was found to be single phase in

Fig. 3. Zr$_{90}$Sn$_{10}$ sample annealed for 680 h at 1073 K: thermogram obtained in calorimetry at 10 K/min and related micrographs showing the microstructure before and after the measurement.

conformity with the proposal of the closure of the miscibility gap at high temperature [5]. The refinement yields a composition of 39.2 at.% Sn, in perfect agreement with the nominal composition, verifying again the reliability of the composition refinement by the Rietveld method.

Finally, the EPMA of the sample at 34 at.% Sn shows that the Sn poor boundary of the η phase is somewhat poorer in Sn (35.8 at.%) than the stoichiometry Zr$_5$Sn$_3$ (37.5 at.%). This analysis is confirmed by the observation of higher values of the lattice parameters. This composition is not accounted by the model Zr$_5$Sn$_{3+x}$ and no model could be established on the basis of the available XRD data. The crystal structure data relative to the η phase are listed in Table 2.

As a conclusion, the presence of a miscibility gap inside the homogeneity domain of the intermetallic phase, as proposed by Kwon and Corbett [5], was confirmed. It is worth noting that this feature is rather exceptional for a binary phase. Another example is uranium carbide with a high-temperature homogeneity domain and ordering at low temperature towards the two compositions UC and UC$_2$ [20].

3.2.3. Determination of the temperature of the peritectoid transformation reaction : $\beta_{Zr} + A15 \to \alpha_{Zr}$

In order to determine the temperature of the peritectoid reaction $\beta_{Zr} + A15 \to \alpha_{Zr}$, the alloy Zr$_{90}Sn_{10}$ was studied by DSC. The oxygen content was measured to be 100 ± 20 wt ppm after either fabrication or annealing treatments. The microstructure was checked before and after the calorimetric tests showing the presence of the same phases. In Fig. 3, the thermogram obtained at 10 K/min is presented. The phase transformation temperature can be derived from the endothermic and exothermic peaks by extrapolation at zero heating and cooling rates. The peritectoid transformation temperature is found to be at 1216 ± 5 K which is 40 K less than the temperature previously proposed in the literature [1,4] and assessed by Abriata et al. [12]. This difference can be attributed to the quite high oxygen content in the alloys studied in the previous works.
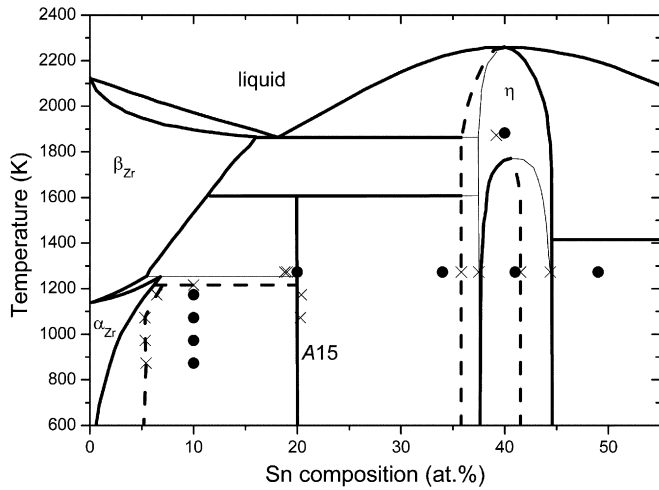
Fig. 4. Zr–Sn phase diagram as redrawn from [5] (full lines), nominal compositions studied in the present experimental work and in Ref. [14] (•), analyzed compositions of the phases (×) and proposed revisions for the phase diagram (dashed lines).

Two other compositions were also studied ($Zr_{86}Sn_{24}$ and $Zr_{82}Sn_{18}$) but the thermograms and the microstructural observations have shown the irreversibility of the phase transformation, illustrated by the precipitation of Zr_5Sn_3. This phenomenon can be attributed to the oxygen pick up during the calorimetric test. The transformation temperatures obtained for these two samples were not taken into account.

The experimental diagram drawn from these measurements is presented in Fig. 4 and compared with the one of Kwon and Corbett [5].

4. Selection of the experimental data

Previous thermodynamic assessments on the Zr–Sn system have been published in Refs. [8–12]. In these assessments, data available until 1992 were used. However, none of the authors considered the η phase with its miscibility gap as reported in Refs. [5,7] or tried to model the defects in the $A15$ phase. The experimental data for the enthalpy of formation of the η phase at Zr_5Sn_3 composition have also been published recently [17]. Furthermore, based on unpublished experimental studies, an assessment including Zr_5Sn_4 has been presented in Ref. [8] and a preliminary assessment of the Zr rich region of Zr–Sn phase diagram was reported in Ref. [12].

Most of the experimental data provided in Refs. [1,2,4] were considered for the present optimization. The values of Sn solubility limit in α_{Zr} in Refs. [1,2,4] are in good agreement with each other. However, recent experiments combined with first-principles calculations have shown that this solubility limit is much higher than the previously accepted one [14]. These data confirmed the earlier statement done by Carpenter et al. [3] and were considered as the most reliable.

At high temperatures, the only data available for the liquid in equilibrium with the β_{Zr} phase are incipient melting measurements [1]. These data were used in the present assessment, together with the reported temperature and composition data for the invariant reactions. However, we used the temperature of the peritectoid reaction $A15 + \beta_{Zr} \leftrightarrow \alpha_{Zr}$ determined in the present work, 1216 ± 5 K, which is 40° lower than the value reported in Ref. [1] and adopted in previous assessments.

Due to the unknown oxygen content in the alloys studied in [1] and the high oxygen content reported in [4], the experimental data obtained for the $(\alpha_{Zr} + \beta_{Zr})/\beta_{Zr}$ boundary [1,4] were low weighted and later rejected for the final optimization.

Table 3
Experimental data considered for the assessment

Type of data	Comment	Reference
Enthalpy of formation of the η phase	Used	[17]
First-principles enthalpy of formation compounds: $A15$, η, $ZrSn_2$	Used	[13]
Enthalpy of mixing in Zr–Sn liquid alloys	Rejected	[15]
	Rejected	[16]
Eutectic and peritectic invariant reactions	Used	[1]
Congruent temperature of η	Used	[1] and [5,6]
Liquidus $+\beta_{Zr}$ domain	Used	[1]
$\alpha + \beta$ domain	Used	[1] and [4]
Peritectoid reaction $A15 + \beta_{Zr} \leftrightarrow \alpha_{Zr}$ (compositions)	Used	[1]
Peritectoid reaction $A15 + \beta_{Zr} \leftrightarrow \alpha_{Zr}$ (temperature)	Used	This work
α_{Zr} solvus	Rejected	[1,2,4]
	Used	[14]
Composition range of $A15$	Used	This work
β_{Zr} solvus	Used	[1]
Composition of the η phase	Used	This work

The data on the phase boundaries $\beta_{Zr}/(\beta_{Zr} + \eta)$ and $\beta_{Zr}/(\beta_{Zr} + A15)$ in Ref. [1] are the only data available and were used in the assessment. The melting points reported for the η phase in Refs. [1,5,6] were also used.

The composition range of the $A15$ phase found in the present work was used together with the compositions measured in the annealed alloys from Ref. [14] where the α_{Zr} solvus was studied.

Concerning the thermodynamic data, the experimental enthalpy of formation of the η phase at the composition Zr_5Sn_3 [17] was used together with the calculated *ab initio* enthalpy values in Ref. [13] for all the intermetallic compounds. However, the *ab initio* value for the η phase was less negative than the experimental one. Consequently, the whole set of *ab initio* values were rescaled relative to the calorimetry data (see Section 6).

The values of the partial enthalpy of mixing in Sn rich alloys measured by calorimetry at 1873 K decreases from −6503 J/mol at 0.58 at.% Zr to −114 470 J/mol at 31.6 at.% Zr after Valishev et al. [15]. This is in opposition to the data of Sudatsova and Batalin [16] which shows that the enthalpy of mixing at 1889 K increases from −172 000 ± 21 J/mol at 0 at.% Zr to −56 000 ± 6 J/mol at 40 at.% Zr. None of these authors reported any particular technique to prevent possible chemical reaction of the melts with the crucible material. In view of the contradictory results none of these data were used during the final optimization procedure.

The list of all the selected data is given in Table 3.

5. Thermodynamic modeling

The Gibbs energy of the pure constituents *i* in phase ϕ is given relative to the element in its stable state at 298.15 K and is denoted by $^0G_i^\varphi$. It is a function of temperature expressed by the power series as shown in Eq. (1). The Scientific Group Thermodata Europe (SGTE) has evaluated the Gibbs energy expression of many pure elements in the temperature range 298.15–6000 K in Ref. [21].

$$^0G_i - H_i^{SER} = a + bT + cT \ln T + \sum_n d_n T^n \tag{1}$$

where $n = 2, 3, -1 \ldots$.

5.1. Substitutional solution phases

All substitutional solution phases i.e. liquid, *bcc* and *hcp* were described using the regular substitutional model. Due to the negligible solubility of Zr in Sn (*bct*) no interaction parameters were evaluated for this phase.

The molar Gibbs energy of formation of a phase ϕ, is determined by the expression

$$G_m^\phi = {}^{ref}G^\phi + {}^{id}G^\phi + {}^{ex}G^\phi \tag{2}$$

where

$$^{ref}G^\phi = x_{Sn}\,{}^oG^\phi_{Sn} + x_{Zr}\,{}^oG^\phi_{Zr} \tag{3}$$

$$^{id}G^\phi = RT(x_{Sn}\ln x_{Sn} + x_{Zr}\ln x_{Zr}) \tag{4}$$

$$^{ex}G^\phi = x_{Sn}x_{Zr}L^\phi_{Sn,Zr} \tag{5}$$

$$L^\phi_{Sn,Zr} = \sum_{n=0}^{N}(x_{Sn} - x_{Zr})^n\,L^{\phi,n}_{Sn,Zr}. \tag{6}$$

$^oG^\phi_{Sn}$ and $^oG^\phi_{Zr}$ are the reference Gibbs energies of the pure components in the structure of ϕ relative to their stable states: *bct* for Sn and *hcp* for Zr. The $^{id}G^\phi$ term is the ideal Gibbs energy contribution due to random mixing of atoms. The $^{ex}G^\phi$ term is the excess term describing deviation from ideality using a regular solution parameter. The regular solution parameter can be made composition dependent by a Redlich–Kister polynomial, Eq. (6). The coefficients $L^{\phi,n}_{Sn,Zr}$ are obtained from least-squares fitting of experimental data. They may be temperature dependent:

$$L^{\phi,n}_{Sn,Zr} = A + BT. \tag{7}$$

Mainly regular interaction parameter i.e. $n = 0$ in Eq. (6), and subregular i.e. $n = 1$ were used and the excess Gibbs energy can be simplified as:

$$^{ex}G^\phi = x_{Sn}x_{Zr}\left[L^{\phi,0}_{Sn,Zr} + (x_{Sn} - x_{Zr})L^{\phi,1}_{Sn,Zr}\right]. \tag{8}$$

5.2. Intermetallic phases

The ZrSn$_2$ phase has the Strukturbericht designation *C*54 with Si$_2$Ti prototype structure [22]. This compound was treated as stoichiometric since there is no experimental information of a homogeneity range. The Gibbs energy of the compound ZrSn$_2$ at temperature T is given relative to the pure constituents i in their stable reference state and multiplied by the stoichiometric coefficient a_i of the constituents i.

$$^OG^\varphi = \sum a_i\,{}^OG^{SER}_i + a + bT + cT\ln T + \cdots. \tag{9}$$

In the A15 phase, two crystallographic sites are occupied (Table 2). We have shown that deviation from the ideal 3:1 composition is accommodated by introducing Zr substitutional defects in the Sn sublattice. Hereafter, it is described using the compound energy formalism (CEF) [23]. The chosen model takes into account this experimental evidence and also the possibility of Sn substitution on Zr sites. It is described as follows:

$$(Sn, \mathbf{Zr})_3(\mathbf{Sn}, Zr)_1. \tag{10}$$

The site occupation of the constituents in different sublattices is given by the site fraction y^s_i and is defined by:

$$y^s_i = N^s_i / N^s \tag{11}$$

where N^s_i is the number of atoms of the constituent i on the sublattice s and N^s is the total number of sites on the sublattice s.

The molar Gibbs energy of the A15 phase is also given by Eq. (2). The term $^{ref}G_m$ now is:

$$^{ref}G = y'_{Sn}y''_{Sn}\,{}^oG_{Sn:Sn} + y'_{Zr}y''_{Zr}\,{}^oG_{Zr:Zr} + y'_{Sn}y''_{Zr}\,{}^oG_{Sn:Zr} + y'_{Zr}y''_{Sn}\,{}^oG_{Zr:Sn}. \tag{12}$$

In Eq. (12), $^oG_{Zr:Sn}$ represents the Gibbs energy of the stoichiometric compound Zr$_3$Sn. The first and last terms represent the pure elements in the A15 structure (lattice stability). These values were taken equal to 8555 J/mol for pure Sn and 12 906 J/mol for pure Zr from *ab initio* calculations leading to the following expression per mole of formula unit:

$$^oG^{A15}_{Sn:Sn} = 4 * (8550 + G^{bct}_{Sn}) \tag{13}$$

$$^oG^{A15}_{Zr:Zr} = 4 * (12\,906 + G^{hcp}_{Zr}). \tag{14}$$

$^oG_{Sn:Zr}$ represents the Gibbs energy of the A15 phase completely filled with anti-structure atoms. It has been determined from other Gibbs energy values using the reciprocal relationship.

^{id}G is the ideal contribution to the molar Gibbs energy assuming random mixing in each sublattice and summing these contributions considering the number of sites and is given by:

$$^{id}G = RT\left[3(y'_{Sn}\ln(y'_{Sn}) + y'_{Zr}\ln(y'_{Zr})) + 1(y''_{Sn}\ln(y''_{Sn}) + y''_{Zr}\ln(y''_{Zr}))\right]. \tag{15}$$

The excess contribution to the molar Gibbs energy is given by

$$^{ex}G = y'_{Sn}y'_{Zr}\left(y''_{Sn}L^0_{Sn,Zr:Sn} + y''_{Zr}L^0_{Sn,Zr:Zr}\right)$$
$$+ y''_{Sn}y''_{Zr}\left(y'_{Sn}L^0_{Sn:Sn,Zr} + y'_{Zr}L^0_{Zr:Sn,Zr}\right)$$
$$+ y'_{Sn}y'_{Zr}(y'_{Sn} - y'_{Zr})\left(y''_{Sn}L^1_{Sn,Zr:Sn} + y''_{Zr}L^1_{Sn,Zr:Zr}\right)$$
$$+ y''_{Sn}y''_{Zr}(y''_{Sn} - y''_{Zr})\left(y'_{Sn}L^1_{Sn:Sn,Zr} + y'_{Zr}L^1_{Zr:Sn,Zr}\right). \tag{16}$$

According to the experimental results in this work and the theoretical treatment in [13] the interaction between the constituents has been described using the L^0 and L^1 Redlich–Kister coefficients for Zr substitutional defects in the Sn sublattice only. Since defects have been observed in only one sublattice, the excess parameters concerning the first sublattice $L(A15, Sn, Zr:Sn)$ and $L(A15, Sn, Zr:Zr)$ have been fixed to zero. It is assumed that the interaction parameters in the second sublattice do not depend on the occupancy of the first sublattice i.e. $L(A15, Sn:Sn, Zr) = L(A15, Zr:Sn, Zr)$. Thus Eq. (16) is simplified to the following expression:

$$^{ex}G = y''_{Sn}y''_{Zr}\left(y'_{Zr}L^0_{Zr:Sn,Zr}\right) + y''_{Sn}y''_{Zr}(y''_{Sn} - y''_{Zr})\left(y'_{Zr}L^1_{Zr:Sn,Zr}\right). \tag{16a}$$

The composition range of the η phase was also described using the CEF. The model was constructed taking into account the crystallographic information given in Table 2, and the experimental evidences. The two Zr sites were merged into one sublattice. Both Sn sublattices were kept: one in which only Sn atoms are allowed and the other one with Sn and vacancies (Va). The model is schematically represented as below:

$$(Zr)_5(Sn)_3(Sn, Va)_1. \tag{17}$$

This model generates two end members at the compositions Zr$_5$Sn$_3$ and Zr$_5$Sn$_4$ with Gibbs energies $^oG_{Zr:Sn:Va}$ and $^oG_{Zr:Sn:Sn}$, respectively. The Gibbs energy is written as follows:

$$G^\eta = y'''_{Va}\,{}^oG_{Zr:Sn:Va} + y'''_{Sn}\,{}^oG_{Zr:Sn:Sn} + RT\left[1(y'''_{Sn}\ln(y'''_{Sn}) + y'''_{Va}\ln(y'''_{Va}))\right]$$
$$+ y'''_{Sn}y'''_{Va}\left[L^0_{Zr:Sn:Sn,Va} + (y'''_{Sn} - y'''_{Va})L^1_{Zr:Sn:Sn,Va}\right]. \tag{18}$$

The ideal and excess contributions to the molar Gibbs energy are due to the random mixing of Sn and vacancies (Va) in the third sublattice.

6. The optimizing procedure and results

All the calculations have been performed using the Thermo-Calc [24] software and the assessment was carried out using its Parrot module.

As already mentioned several thermodynamic assessments on this system has been published. In Fig. 5 some of the earlier assessed phase diagrams are reproduced. One may note the different descriptions of the liquidus on the Sn rich side, the reason being the lack of experimental information.

In the assessment by Roberti [8] the miscibility gap in the η phase was not considered, instead the Zr$_5$Sn$_3$ and Zr$_5$Sn$_4$ were modeled as two stoichiometric phases, separated by a two phase
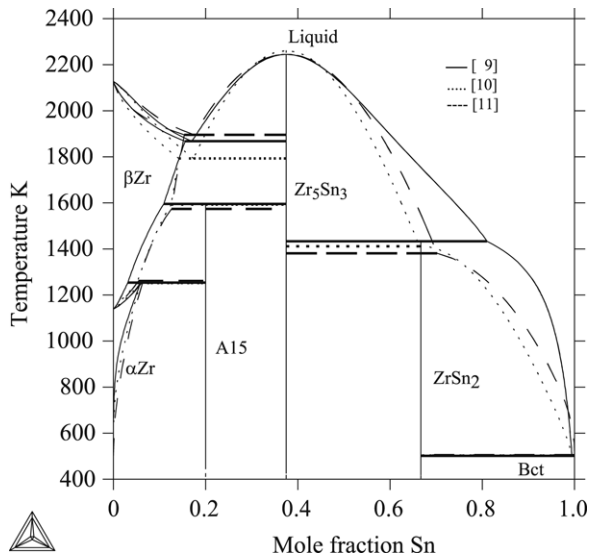
Fig. 5. Previous thermodynamic assessments of the Zr–Sn binary system performed by Korb et al. [9], Subasic [10] and Dupin et al. [11].
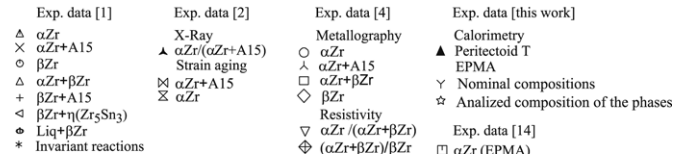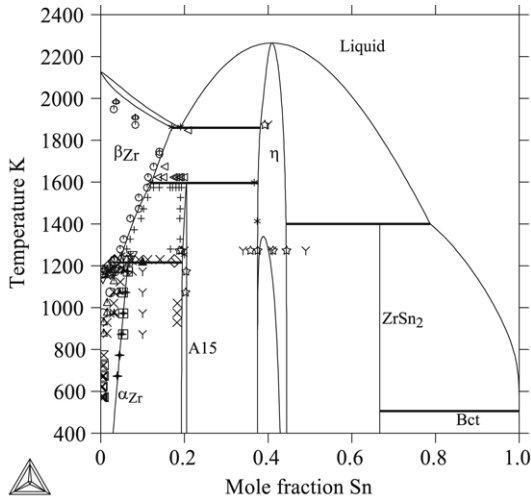

Fig. 6. Optimized Zr–Sn phase diagram [this work] compared with experimental data and first-principles calculations.

Fig. 7. Blow-up of the Zr rich corner of the assessed Zr–Sn binary system compared with experimental data and first-principles calculations.

system. The composition at higher Zr content was accommodated by allowing a high fraction of anti-site defect only in the Sn sublattice and using both regular and subregular excess terms. The asymmetrical nature of the L^1 parameter makes the $A15$ phase stable at Zr richer content.

The agreement between the assessed phase diagram and the experiments is shown in Figs. 6 and 7. The liquidus in equilibrium with β_{Zr} has been assessed at a much higher value than the experiments of Ref. [1]. It was very difficult to fit the experimental eutectic temperature together with these data. As they do not seem to be compatible, we chose to put a higher weight on the eutectic temperature. However Dupin et al. [11] managed to obtain a better description of the tie-line liquid $+\beta_{Zr}$.

Concerning the enthalpy data, Dupin et al. [11] used the estimated enthalpies obtained after Miedema's model [25] and we use the *ab initio* enthalpies. Since Miedema's enthalpies are more negative than the *ab initio* values we use in the present work, a variation in the stability of the phases and their interaction parameters should be expected. In Table 4, Miedema's enthalpy values in comparison with the experimental value for the η phase and the calculated *ab initio* enthalpies are reported.

The whole set of *ab initio* calculated enthalpies was rescaled relative to the only experimental point available [17]. Thus, the ratio between the experimental enthalpy of formation of the Zr_5Sn_3 compound i.e. $-71\,200$ J/mol and its *ab initio* value i.e. $-55\,670$ J/mol, was used as rescaling coefficient (RC) equal to 1.2789. Note that the original *ab initio* values from Ref. [13] are given in Table 4. Those values are then multiplied by RC and used as enthalpies used in the assessment. Thereby, we hope to cancel the systematic errors that are always present in *ab initio* calculations, due to the approximations used. For instance, in *ab initio* calculations the electronic-ion interaction is described by different methods and the potential obtained for this interaction is either truncated (Pseudopotential) or not (Full potential) [26,27]. The rescaled *ab initio* values still contain the structure-dependent contributions to phase stability, which are ignored in Miedema's

region throughout the whole temperature range and the Zr_5Sn_4 compound is described with a peritectic decomposition.

The presently assessed phase diagram is drawn in Fig. 6. One of the main improvements of the description consists of the introduction of the η phase with a miscibility gap. This was achieved by introducing a positive temperature dependent excess term for $L^0_{Zr:Sn:Sn,Va}$ to describe the miscibility gap and a negative excess term for $L^1_{Zr:Sn:Sn,Va}$ which allows to describe its asymmetrical shape (Fig. 6). However, the model proposed in the present assessment, $(Zr)_5(Sn)_3(Sn, Va)_1$ does not describe the Sn poor limit obtained in Section 3.

The modeling of the non-stoichiometry of the $A15$ phase by anti-site defects is another contribution to the study of this binary
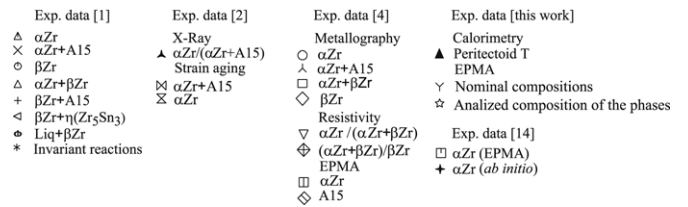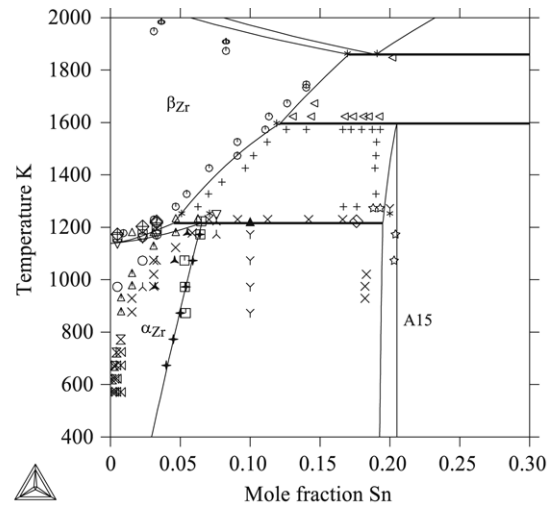
Table 4
Enthalpy of formation of the stable intermetallic compounds in the Zr–Sn binary system

Compound	ΔH_{form} (J/mol)	Reference
(Zr_4Sn)[a]	−29 940	FP [13]
	−38 292	FP [13] (scaled)
	−42 667	Optimized (this work)
	−58 898	Optimized [11]
	−48 082	Miedema [25]
Zr_5Sn_3	−55 670	FP [13]
	−71 200	FP [13] (scaled)
	−74 345	Optimized (this work)
	−81 551	Optimized [11]
	−71 200	DRC, T=1473 K [17]
	−80 960	Miedema [25]
Zr_5Sn_4	−58 490	FP [13]
	−74 806	FP [13] (scaled)
	−79 115	Optimized (this work)
	−85 989	Miedema [25]
$ZrSn_2$	−42 905	FP [13]
	−54 874	FP [13] (scaled)
	−56 270	Optimized (this work)
	−72 639	Optimized [11]
	−67 370	Miedema [25]

Used method: Miedema, First Principles (FP), Thermo_Calc (optimized), experimental method (DRC).

[a] The first-principles calculation of this phase corresponds to an alloy where Zr substitution on the Sn has the configuration $Zr_{48}(Sn_{13}Zr_3)$ and has the stoichiometry (79.7 at.%Zr) close to that of the Zr_4Sn compound (80 at.% Zr). See text.

model. Miedema's method represents a parametrized atom model which systematizes the data base available for alloy formation [25]. So it seems a natural choice to replace missing experiments with the *ab initio* values. Rescaling those values is an unusual procedure, but it helps to take the *ab initio* data into account, meanwhile the only available thermodynamic information on the enthalpy of formation of the η phase is considered to be the most reliable.

A blow-up of the Zr rich part of the assessed phase diagram is shown in Fig. 7. One may observe that the α_{Zr} solvus has been fitted in agreement with the experiments and the *ab initio* calculations by Toffolon et al. [14]. The $\alpha_{Zr}/(\alpha_{Zr}+\beta_{Zr})$ boundary is at slightly lower temperature than the experiments in [1,2,4].

Concerning the liquid phase, the excess terms were evaluated by using two Redlich–Kister coefficients $L^0_{Sn,Zr}$ and $L^1_{Sn,Zr}$. Due to limited experimental data for the liquid phase, only L^0 has been made temperature dependent. Our description of the thermodynamic data of the liquid phase follows better the experimental partial enthalpy of Zr in Ref. [16] than that in [15], as shown in Fig. 8. At the Zr rich corner, the liquid from Ref. [11] is more stable than the liquid described in the present work. However as the zirconium content decreases, the agreement between both assessments and the experimental data becomes better. This is due to the lack of information over the entire liquid region and the
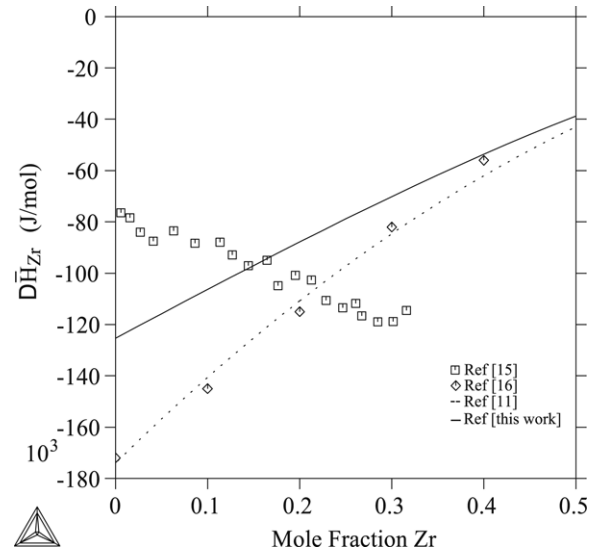

Fig. 8. Calculated partial enthalpy of Zr in liquid Sn at 1889 K [this work] (continuous line) and Dupin et al. [11] (dashed line) compared with experimental data [15,16].

different choice made by the assessors concerning the enthalpy data.

The excess terms of the β phase were evaluated with two Redlich–Kister coefficients $L^0_{Sn,Zr:Va}$ and $L^1_{Sn,Zr:Va}$ both of them temperature dependent. The α phase was described with three excess terms. In Table 5 the characteristics of the assessed invariant reactions in the Zr–Sn binary system are presented and compared with the available experimental data. In Table 6 all the parameters optimized in this work are listed. Note that the description for pure elements GHSERZr and GHSERSn is taken from A. T. Dinsdale in Ref. [21].

7. Conclusion

This paper has provided an important contribution to a better understanding of the Zr–Sn binary system thanks to the experimental studies.

The most important findings are the following:

- The non-stoichiometry of the $A15$ phase has been confirmed and explained by the presence of Zr substitutional defects in the Sn sublattice.
- The region Zr_5Sn_3–Zr_5Sn_4 was re-examined. At 1873 K, a single phase (η) was found, with a composition variation. At 1273 K, the existence of a miscibility gap was confirmed. The homogeneity range was found to extend from 35.8 at.% Sn to 37.5 at.% Sn on the Zr rich side and 41.2 at.% to 44.4 at.% on the Sn rich side.

Table 5
Zr–Sn binary system: invariant reactions compared with those in the literature

Reaction	Composition at.% (Sn)			Temperature (K)	Reaction type	Reference
Liq $\leftrightarrow \beta_{Zr} + \eta$	19.1	17.0	37.5	1863 ± 15	Eutectic	[1]
	19.0	17.1	38.1	1859		This work
$\beta_{Zr} + \eta \leftrightarrow A15$	12.0	37.5	20.0	1598 ± 20	Peritectoid	[1]
	12.1	37.6	20.5	1596		This work
$\beta_{Zr} + A15 \leftrightarrow \alpha_{Zr}$	5.1	20.0	7.1	1253 ± 20	Peritectoid	[1]
				1216 ± 5		This work, exp.
	4.5	19.5	6.5	1216		This work, opt.
$\eta + Liq \leftrightarrow ZrSn_2$	36.7	78.96	66.7	1413 ± 15	Peritectic	[1]
	44.3	78.76	66.7	1400		This work
$\eta \leftrightarrow Liq$	37.5			2258 ± 25	congruent	[1]
	41.2			2263		[5]
	39.8			2265		This work

Table 6
List of the functions used in this work and optimized parameters in (J/mol) and Temperature (K)

Phase	Functions	Temperature range	Reference
Liquid			
L(liquid, Sn, Zr; 0)	$-140\,175.16 - 14.09329 * T$	$100 < T < 3000$	[This work]
L(liquid, Sn, Zr; 1)	$14\,799.442$	$100 < T < 3000$	[This work]
BCC_A2			
2 sublattices sites 1 3 constituents **Zr**, **Sn**:Va			
L(bcc_A2, Sn, Zr:Va; 0)	$-112\,959.92 - 34.81672 * T$;	$100 < T < 3000$	[This work]
L(bcc_A2, Sn, Zr:Va; 1)	$53\,075.36 - 29.643272 * T$;	$100 < T < 3000$	[This work]
HCP_A3			
3 sublattices sites 1 1 1 constituents **Zr**, **Sn** : Va :Va			
G(hcp_A3, Sn:Va:Va; 0)	$3900 - 7.646 * T + $ GHSERSn	$100.00 < T < 3000$	[21]
L(hcp_A3, Sn, Zr:Va:Va; 0)	$-148\,022.5 + 19.4074 * T$	$298.15 < T < 6000$	[This work]
L(hcp_A3, Sn, Zr:Va:Va; 1)	$173\,681.886 - 21.9121 * T$	$298.15 < T < 6000$	[This work]
L(hcp_A3, Sn, Zr:Va:Va; 2)	$104\,271.96$	$298.15 < T < 6000$	[This work]
A15			
2 sublattices sites 3 1 Sn, **Zr:Sn**, **Zr**			
G(A15, Sn:Sn; 0)	$4 * (8550 + $ GHSERSn$)$	$298.15 < T < 6000$	[This work]
G(A15, Zr:Sn; 0)	$-195\,357.79 + 15.565 * T + 3 *$ GHSERZr $+$ GHSERSn	$298.15 < T < 6000$	[This work]
G(A15, Sn:Zr; 0)	$195\,357.79 - 15.565 * T + 3 *$ GHSERSn $+$ GHSERZr	$298.15 < T < 6000$	[This work]
G(A15, Zr:Zr; 0)	$4 * (12\,906 + $ GHSERZr$)$	$298.15 < T < 6000$	[This work]
L(A15, Zr:Sn, Zr; 0)	$-79\,959.713 + 20.00604 * T$;	$298.15 < T < 6000$	[This work]
L(A15, Zr:Sn, Zr; 1)	$-99\,146.4844$	$298.15 < T < 6000$	[This work]
η phase			
3 sublattices sites 5 3 1 constituents **Zr:Sn :Sn**, **Va**			
G(η, Zr:Sn:Sn; 0)	$-712\,020.91 + 54.8483 * T+$ $5 *$ GHSERZr $+ 4 *$ GHSERSn	$298.15 < T < 6000$	[This work]
G(η, Zr:Sn:Va; 0)	$-594\,759.92 + 44.362516 * T$ $+5 *$ GHSERZr $+ 3 *$ GHSERSn	$298.15 < T < 6000$	[This work]
L(η, Zr:Sn:Sn, Va; 0)	$20\,000.0 - 28 * T$		[This work]
L(η, Zr:Sn:Sn, Va; 1)	$-73\,000.00 + 33.0 * T$		
ZrSn$_2$ 2 sublattices sites 1 2 constituents **Zr**; **Sn**			
G(ZrSn$_2$, Zr:Sn, Zr; 0)	$-168\,810.61 + 11.839315 * T$	$298.15 < T < 6000$	[This work]

- The temperature of the peritectoid reaction $\beta_{Zr} + A15 \leftrightarrow \alpha_{Zr}$ was measured at 1216 K, 40 K below the previously reported values.

The Zr–Sn binary system was reassessed taking into account these new information. In particular, the models for η and $A15$ phases were chosen in agreement with the crystallography. *Ab initio* enthalpies of formation for all the intermetallic phases and previous experimental information on this system were also considered in the assessment.

Acknowledgements

References

[1] D.J. McPherson, M. Hansen, Trans. ASM. 45 (1953) 915–933.
[2] G.R. Speich, S.A. Kulin, Am. Soc. Metals (1953) 197–207.
[3] G.J.C Carpenter, E.F. Ibrahim, J.F. Watters, J. Nucl. Mater. 102 (1981) 280–291.
[4] D. Arias, L. Roberti, J. Nucl. Mater. 118 (1983) 143–149.
[5] Y.-U. Kwon, J.D. Corbett, Chem. Mater. 2 (1990) 27–33.
[6] Y.-U. Kwon, J.D. Corbett, Chem. Mater. 4 (1992) 187–190.
[7] Y.-U. Kwon, J.D. Corbett, Chem. Mater. 4 (1992) 1348–1355.
[8] L. Roberti, in: I. Ansara (Ed.) Proceeding of the CALPHAD XXIII Meeting, Grenoble, France, 1999.
[9] J. Korb, K. Hack, in: I. Ansara, A. Dinsdale, M.H. Rand (Eds.), Thermochemical Database for Light Alloys, 1998.
[10] N. Subasic, CALPHAD 22 (2) (1998) 157–165.
[11] N. Dupin, I. Ansara, C. Servant, C. Toffolon, C. Lemaignan, J.C. Brachet, J. Nucl. Mater. 275 (1999) 287–295.
[12] J.P. Abriata, J.C. Bolcich, D. Arias, Bull. Alloy Phase Diag. 4 (2) (1983) 147–154.
[13] V.I. Baykov, R. Jerlerud Pérez, P.A. Korzhavyi, B. Sundman, B. Johansson, Scr. Mater. 55 (2006) 485–488.
[14] C. Toffolon-Masclet, J.C. Brachet, C. Servant, J.-M. Joubert, P. Barberis, N. Dupin, P. Zeller, Zirconium in Nuclear Industry, 15th. ASTM Int. Symp. June 24–28, 2007, Sunriver, Oregon USA.
[15] M.G. Valishev, O.Yu. Sidorov, S.P. Kolesnikov, P.V. Gerl'd, Izvest. Akad. Nauk SSSR, Metal. 4 (1992) 46–50.
[16] V.S. Sudatsova, G.I. Batalin, Rasplavy 1 (1990) 88–90.
[17] S.V. Meschel, O.J. Kleppa, Therm. Acta 314 (1998) 205–212.
[18] G. Grand, S. Andersson, Acta. Chem. Scand. 1 (1960) 956–957.
[19] H.L. Luo, E. Vielhaber, Z. Physik 230 (1970) 443–448.
[20] R. Benzl, C.G. Hoffman, G.N. Ruppert, High Temperature Sci. 1 (1969) 342–359.
[21] A.T. Dinsdale, CALPHAD 15 (1991) 317–425.
[22] P. Villars, L.D. Calvert (Eds.), Pearson's Handbook of Crystallographic Data for Intermetallic Phases, American Society of Metals, Metals Park, Ohio, 1985.
[23] B. Sundman, J. Ågren, J. Phys. Chem. Solids 42 (1981) 297–301.
[24] B. Sundman, CALPHAD 8 (1984) 104–108.
[25] F. De Boer, R. Boom, W.C.M. Mattens, A.R. Miedema, A.K. Niessen, in: D.G. Pettifor (Ed.), Cohesion in Metals, vol. 1, North Holland, Amsterdam, 1988.
[26] I.A. Abrikosov, A.M.N. Niklasson, S.I. Simak, B. Johansson, A.V. Ruban, H.L. Skriver, Phys. Rev. Lett. 76 (1996) 4203–4206.
[27] J.P. Perdew, Y. Wang, Phys. Rev. B 45 (1992) 13244–13249.